

Production and Transfer of Energy and Information in Hamiltonian Systems

Ch. G. Antonopoulos^{1,*}, E. Bianco-Martinez¹, M. S. Baptista¹

1 Department of Physics/ICSMB, University of Aberdeen, Aberdeen, United Kingdom

* E-mail: chris.antonopoulos@abdn.ac.uk

Abstract

We present novel results that relate energy and information transfer with sensitivity to initial conditions in chaotic multi-dimensional Hamiltonian systems. We show the relation among Kolmogorov-Sinai entropy, Lyapunov exponents, and upper bounds for the Mutual Information Rate calculated in the Hamiltonian phase space and on bi-dimensional subspaces. Our main result is that the net amount of transfer from kinetic to potential energy per unit of time is a power-law of the upper bound for the Mutual Information Rate between kinetic and potential energies, and also a power-law of the Kolmogorov-Sinai entropy. Therefore, transfer of energy is related with both transfer and production of information. However, the power-law nature of this relation means that a small increment of energy transferred leads to a relatively much larger increase of the information exchanged. Then, we propose an “experimental” implementation of a 1-dimensional communication channel based on a Hamiltonian system, and calculate the actual rate with which information is exchanged between the first and last particle of the channel. Finally, a relation between our results and important quantities of thermodynamics is presented.

Author Summary

1 Introduction

After the pioneering work by Shannon [1] on information, it became clear that it is a very useful and important concept as it can measure the amount of uncertainty an observer has about a random event and thus provides a measure of how unpredictable it is. The degree of disorder of a chaotic dynamical system is related to the degree of its chaotic behavior which is, in turn, characterized by the rate of exponential divergence of neighboring initial conditions, that is by the magnitude of the positive Lyapunov

exponents [2]. It is the sensitive dependence on initial conditions [2–4] that produces information since two different but indistinguishable initial conditions at a certain precision will evolve into distinguishable states after a finite time [3]. This relation between production of information and sensitive dependence was made clear for systems that have absolutely continuous conditional measures [5, 6], by:

$$H_{\text{KS}} = \sum_i \lambda_i, \quad (1)$$

where H_{KS} represents the Kolmogorov-Sinai or KS entropy (Shannon’s entropy per unit of time) and λ_i are the positive Lyapunov exponents of the dynamical system [2, 3, 7, 8], which measure how sensitive to initial conditions the system is. This is a property that has been found to be true for many dynamical systems [3]. In general, for bounded systems $H_{\text{KS}} \leq \sum_i \lambda_i$, $\lambda_i > 0$ [9].

Energy and information can be produced in a system or transferred between its different “parts” or “constituents” [10–12]. If transferred, there are always at least two “entities” involved. In general, they can be nodes, modes, or related functions that can be defined on subspaces or projections of the phase space of the system.

Another related concept to the Shannon entropy that can characterize random complex systems is the Mutual Information (MI) [1] which is a measure of how much uncertainty one has about a state variable after observing another state variable. For deterministic systems that present correlations, a more appropriate quantity for measuring the transfer of information is the Mutual Information Rate (MIR), MI per unit of time. In Refs. [10, 13–15], the authors have developed alternative methods to overcome problems that stem from the definition of probabilities for these quantities and proposed the use of bounds for the MIR. In Ref. [10], the authors have derived an upper bound for the MIR between two nodes or two groups of nodes that depend on the largest Lyapunov exponents of the subspace of the network formed by the nodes. In particular, they have showed that:

$$\text{MIR} \leq I_c = l_1 - l_2, \quad l_1 \geq l_2, \quad (2)$$

where l_1 and l_2 are the two finite time and size Lyapunov exponents calculated in the bi-dimensional observation space which for simplicity will be referred herein as the Lyapunov exponents of the bi-dimensional subspace. In our study, when the observation space is formed by the kinetic (K) and

potential (P) energy variables of the Hamiltonian, then the upper bound for the MIR in the KP space $I_c^{KP} = \lambda_1^{KP} - \lambda_2^{KP}$ (i.e. $l_1 = \lambda_1^{KP}$ and $l_2 = \lambda_2^{KP}$) represents the upper bound for the information transferred per unit of time between the kinetic and potential energies. The use of the KP space to study the relationship between energy and information exchange is justifiable because the transfer of energy from kinetic to potential energy is easy and well understood. However, we will also study this relationship in other bi-dimensional subspaces such as those formed by any two nodes of the Hamiltonian system.

The main result of our work is Eq. (26), which states that when considering specific energy subintervals, the time rate of energy transferred from the kinetic to the potential variable during a time step is a power-law function of either the largest Lyapunov exponent λ_1 of the Hamiltonian or of the upper bound I_c^{KP} for the MIR of the bi-dimensional KP space.

We then present the generalization of these power-law relations when considering much larger energy intervals of chaotic behavior with initial conditions set initially in different parts of the phase space of the same Hamiltonian system. We also consider different Hamiltonian systems in which we illustrate how they can be used to create communication systems.

The second main result is Eq. (38) which states that the upper bound for the MIR exchanged between the potential and kinetic energy is smaller than the upper bound for the MIR between two groups of oscillators formed each by half the oscillators of the Hamiltonian, and this is in turn smaller than the whole time rate of information produced by the system expressed by H_{KS} . We provide a proof of this result in the Appendix. This result implies that, when one observes a Hamiltonian system through its kinetic and potential energy (i.e. in its KP space), one should not expect to have more information about the Hamiltonian system than when observing it directly (i.e. by observing half of its nodes or all of its variables).

The relation among energy, entropy, and information is a long lasting problem in physics. Nineteenth century saw the discovery of the two laws of thermodynamics, almost happening at the same time. The first law relates the rate of change of the energy of a body with the heat and work produced and the second, the rate of the change of the entropy of the body with the heating, implying the growth of its entropy during an adiabatic and irreversible process. Thermodynamics turned out to be a very important mathematical theory that can describe successfully macroscopic systems in equilibrium, based on the thermodynamic laws and provides a link between work, energy, and entropy as a universal competition,

i.e. when a body approaches equilibrium, energy tends to a minimum and entropy to a maximum (see for example Ref. [16]).

In 1929, after a long lasting controversy, Leó Szilárd [17] and more recently the authors in Refs. [18,19], showed that Maxwell’s hypothetical demon does not contradict the second law of thermodynamics, implying that in principle one can convert information to free energy. By free energy we mean the portion of the energy of a system that is available to perform work mediated by thermal energy. It was only very recently in 2010 [20], that an experimental demonstration of this information to energy conversion has been achieved.

In Ref. [11], the authors study the energy transfer in terms of the classical dynamics of two particles that move in harmonic potential wells, interacting with the same external environment of N noninteracting chaotic systems. They found that the oscillators can exchange energy through the environment when in almost-perfect resonance and in Ref. [12], a simple and solvable model of a device that transfer energy from a cold to a hot system by rectifying thermal fluctuations is presented. In order for this to happen, the device requires a memory register to which it can write information. The subtle issue of the connection between work and information processing is presented in Ref. [21] in a solvable model of an autonomous Maxwell’s demon. The authors studied and explained a device that makes measurements about the system states, stores this information into a register, and delivers work by rectifying thermal fluctuations.

In this work however, we are interested in providing the relation between energy transfer and information production and transfer in multi-dimensional chaotic Hamiltonian systems, e.g. in isolated systems where the total energy of the system remains constant and no exchange of heat or matter with the surroundings exists. Such a relation could allow one to realize how much information a sort of Maxwell’s demon would need in order to be able to transfer a certain amount of energy between oscillatory modes in Hamiltonian systems. Hamiltonian systems such as those we study herein differ from thermodynamic systems in the sense they are far from the thermodynamic limit, i.e. they have a small dimensionality. However, in the Discussion session, we provide a link between our results and important quantities of thermodynamics.

The paper is organized as follows: In Sec. 2 we present the basic material needed in our study. This includes the presentation of the two Hamiltonian systems and some of its important properties, the definition of the KP bi-dimensional observation space and a brief discussion about important quantities

from the theory of information such as upper bound for MIR and KS entropy. In Subsec. 3.1, we present the relation between the largest Lyapunov exponent of the Hamiltonian system and that of the bi-dimensional space of the kinetic and potential energy. Then, in Subsec. 3.2, we explain how one can arrive at Eq. (26) about the relation between production and transfer of information when considering specific energy subintervals of chaotic behavior. In Subsec. 3.3 we generalize the main results of our study by considering the case of different Hamiltonian systems for much larger energy intervals and with initial conditions set in different parts of the phase space of the systems. Then, in Sec. 4 we illustrate how one can implement a 1-dimensional communication channel based on a Hamiltonian system, and calculate the actual rate with which information is exchanged between the first and last particle of the channel. In the Discussion section we briefly recall the main results of our study, their implications and relation with quantities of thermodynamics. Finally, in the Appendix we provide a proof of the inequality presented in Eq. (38).

2 Materials and Methods

2.1 Fermi-Pasta-Ulam Hamiltonian

In this work we use two different Hamiltonian systems. We first consider the 1-dimensional lattice of N particles with equal masses and nearest neighbour interactions with quartic nonlinearities (β -model) given by the Fermi-Pasta-Ulam (FPU) Hamiltonian [22]:

$$H(x, \dot{x}) = \frac{1}{2} \sum_{j=1}^N \dot{x}_j^2 + \sum_{j=0}^N \left(\frac{1}{2} (x_{j+1} - x_j)^2 + \frac{1}{4} \beta (x_{j+1} - x_j)^4 \right) = E \quad (3)$$

adopting fixed boundary conditions:

$$x_0(t) = x_{N+1}(t) = 0, \forall t.$$

Here, x_j and \dot{x}_j is the position and conjugate momentum of the j th particle, respectively.

For this system, we use initial conditions in the neighborhood of two particular simple periodic orbits of (3) which are called SPO1 and SPO2 [23,24]. The reason for this choice is that they allow us to control in a systematic way the increase of the energy of the system so that chaotic motion will be sustained.

Any other way of increasing the energy of the system so that chaotic behavior can exist may be equally used as well.

SPO1 is specified by the conditions:

$$x_{2j}(t) = 0, \quad x_{2j-1}(t) = -x_{2j+1}(t) \equiv \hat{x}(t), \quad j = 1, \dots, \frac{N-1}{2}, \quad (4)$$

and exists for all odd N , keeping every even particle stationary at all times. It is not difficult to show that this is, in fact, the $q = (N+1)/2$ mode of the linear lattice (i.e. $\beta = 0$) with frequency $\omega_q = \sqrt{2}$. The remarkable property of this solution is that it is continued in precisely the same spatial configuration in the nonlinear lattice as well, due to the form of the equations of motion associated with Hamiltonian (3):

$$\ddot{x}_j(t) = x_{j+1} - 2x_j + x_{j-1} + \beta \left((x_{j+1} - x_j)^3 - (x_j - x_{j-1})^3 \right), \quad j = 1, \dots, N \quad (5)$$

which reduce, upon using (4) with the fixed boundary conditions to a single second order nonlinear differential equation for $\hat{x}(t)$:

$$\ddot{\hat{x}}(t) = -2\hat{x}(t) - 2\beta\hat{x}^3(t) \quad (6)$$

describing the oscillations of all moving particles of SPO1, with $j = 1, 3, 5, \dots, N$. For the stationary particles (i.e. $j = 2, 4, 6, \dots, N-1$) we have $\hat{x}(t) = 0, \forall t \geq 0$. The solution of (6) is well known in terms of Jacobi elliptic functions [25] and can be written as:

$$\hat{x}(t) = C \operatorname{cn}(\lambda t, \kappa^2), \quad (7)$$

where:

$$C^2 = \frac{2\kappa^2}{\beta(1-2\kappa^2)}, \quad \lambda^2 = \frac{2}{1-2\kappa^2}, \quad (8)$$

and κ^2 is the modulus of the cn elliptic function. The energy per particle of SPO1 is then found to be:

$$\frac{E}{N+1} = \frac{1}{4}C^2(2 + C^2\beta) = \frac{\kappa^2(1-\kappa^2)}{\beta(1-2\kappa^2)^2} \quad (9)$$

by substituting simply the solution $\hat{x}(t)$ of Eq. (7) in Hamiltonian (3).

SPO2 is defined in a similar way. In particular, it exists for $N = 5 + 3m$, $m = 0, 1, 2, \dots$ and

corresponds to the case where every third particle is fixed, while the two in between move in opposite directions (in an out of phase fashion). Following similar arguments as for the SPO1 mode, the energy per particle of SPO2 is given by [23]:

$$\frac{E}{N+1} = \frac{2\kappa^2(1-\kappa^2)}{3\beta(1-2\kappa^2)^2}.$$

We treat E as a control parameter for the chaoticity of the FPU system (3). From now on, we drop the time-dependence notation of all involved variables for simplicity but use it wherever is needed.

2.2 Bose-Einstein condensate Hamiltonian

The second Hamiltonian system we use in this paper is the Bose-Einstein Condensate (BEC) model [24] which is given by:

$$H = \frac{1}{2} \sum_{j=1}^N (\dot{x}_j^2 + x_j^2) + \frac{1}{8} \sum_{j=1}^N (\dot{x}_j^2 + x_j^2)^2 - \frac{1}{2} \sum_{j=1}^N (\dot{x}_j \dot{x}_{j+1} + x_j x_{j+1}), \quad (10)$$

where x_j , \dot{x}_j is the position and conjugate momentum of the j th particle (i.e. boson), respectively.

It possesses the second integral of motion:

$$F = \sum_{j=1}^N (\dot{x}_j^2 + x_j^2), \quad (11)$$

and therefore chaotic behavior can only occur for $N \geq 3$.

We impose periodic boundary conditions in Eq. (10):

$$\begin{aligned} x_{N+1}(t) &= x_1(t) \text{ and} \\ \dot{x}_{N+1}(t) &= \dot{x}_1(t), \forall t, \end{aligned} \quad (12)$$

and use, for the same reason as in the FPU case, initial conditions set in the neighborhood of the out-of-phase mode (OPM):

$$\begin{aligned} x_j(t) &= -x_{j+1}(t) \equiv \hat{x}(t), \\ \dot{x}_j(t) &= -\dot{x}_{j+1}(t) \equiv \dot{\hat{x}}(t), \forall j = 1, \dots, N \end{aligned} \quad (13)$$

with N being even.

2.3 Observation subspaces and quantities calculated on them

The FPU system (3) can be simply written in the form:

$$H = K + P = E = \text{const} \quad (14)$$

where:

$$\begin{aligned} K &= \frac{1}{2} \sum_{j=1}^N \dot{x}_j^2 \text{ and} \\ P &= \sum_{j=1}^N \left(\frac{1}{2} (x_{j+1} - x_j)^2 + \frac{1}{4} \beta (x_{j+1} - x_j)^4 \right). \end{aligned} \quad (15)$$

However, the BEC system (10) is not written in the same form and this will allow us to generalize the results of our study in the case where the KP space is not implied directly by the Hamiltonian form.

In our analysis, we define and study quantities like Lyapunov exponents initially in the bi-dimensional KP space, since K is a meaningful physical quantity. Potential energy can be easily measured as well or estimated since $P = E - K$. However, we also consider the (x_1, x_N) observation space which is constructed by the position coordinates of the first and last particle of the Hamiltonian. For the FPU case, we know that:

$$\frac{dH}{dt} = \frac{dK}{dt} + \frac{dP}{dt} = 0, \quad (16)$$

where:

$$\begin{aligned} \frac{dK}{dt} &= \sum_{j=1}^N \dot{x}_j \ddot{x}_j \text{ and} \\ \frac{dP}{dt} &= \sum_{j=1}^N \left[(\dot{x}_{j+1} - \dot{x}_j) [(x_{j+1} - x_j) + \beta (x_{j+1} - x_j)^3] \right]. \end{aligned} \quad (17)$$

Equation (16) is valid since the FPU Hamiltonian (3) is a global integral of the motion and thus a conserved quantity during time evolution.

Along the lines of ideas presented in Ref. [10], we compute the upper bound I_c for the MIR between

any two groups of $N/2$ nodes each. The upper bound I_c for the MIR is defined as (see supplementary material in Ref. [10]):

$$I_c = 2 \sum_{i=1}^{\tilde{N}} \tilde{\lambda}_i - \tilde{H}_{\text{KS}} = 2\tilde{H} - \tilde{H}_{\text{KS}}, \quad (18)$$

where \tilde{N} is half the number of positive Lyapunov exponents measured in the subspace. Naturally, $\tilde{N} \leq N/2$. However, for the simulations we have performed we have set $\tilde{N} = N/2$. So, $\tilde{\lambda}_i$, $i = 1, \dots, N$ represent the greater than or equal to zero Lyapunov exponents of the N -dimensional projection constructed using scalar time series x_i , for $i = 1, \dots, N$, which can be calculated in many ways, for example by calculating the finite size and finite time Lyapunov exponents or expansion rates [10]. $\tilde{H}_{\text{KS}} = \sum_{i=1}^N \tilde{\lambda}_i$ represents the sum of all greater than or equal to zero Lyapunov exponents of the projection (i.e. an approximation for the KS entropy) and $\tilde{H} = \sum_{i=1}^{\tilde{N}} \tilde{\lambda}_i$. Herein, we estimate them by computing the Lyapunov exponents of the Hamiltonian following [7, 8] and by keeping only those that are positive.

We also need to compute the upper bound I_c^{KP} for the MIR in the bi-dimensional KP space representing the maximum information exchanged between the kinetic (K) and potential (P) energies. Using the ideas from Ref. [10], I_c^{KP} is given by:

$$I_c^{KP} = \lambda_1^{KP} - \lambda_2^{KP} \quad (19)$$

where λ_1^{KP} and λ_2^{KP} are the two positive Lyapunov exponents of the KP space with $\lambda_1^{KP} > \lambda_2^{KP}$. In the case where $\lambda_2^{KP} \leq 0$, we have $I_c^{KP} = \lambda_1^{KP}$ and thus it turns out that $\text{MIR}^{KP} \leq \lambda_1^{KP}$ (see Ref. [10]).

In a series of papers [24, 26–31], the authors report for dynamical systems ranging from different kinds of billiards to multi-dimensional Hamiltonian systems, that the largest Lyapunov exponent λ_1 of the system scales with the energy E with a power-law of the form:

$$\lambda_1 \propto E^b \quad (20)$$

where b is a real positive constant. This power-law dependence is valid for a rather large energy interval that can support chaotic behavior.

To numerically calculate $\frac{dK}{dt}$ we use:

$$\frac{dK}{dt} \approx \frac{K(t) - K(t - dt)}{dt} = \frac{\Delta K}{dt}$$

from which we can define the time average of the absolute value of the transfer of kinetic energy per unit of time through:

$$\left\langle \left| \frac{dK}{dt} \right| \right\rangle_t \approx \left\langle \left| \frac{\Delta K}{dt} \right| \right\rangle_t, \quad (21)$$

where $\langle \cdot \rangle_t$ denotes the time average over the integration of the trajectory $\vec{X}(t)$ up to $t = t_f$. $|\cdot|$ is the absolute value of the argument and we use it because we want to relate the quantities of Eq. (21) to positive average quantities, such as the positive Lyapunov exponents. Accordingly, ΔK is the amount of kinetic energy being transferred between K and P during a time step.

Since the BEC Hamiltonian (10) is not of the form $H = K + P$ as the FPU system, we reside on the calculation of a similar quantity $\langle \left| \frac{\Delta K_1}{dt} \right| \rangle_t$ based on the kinetic energy of any of its particles, for example of the first particle x_1 :

$$\left\langle \left| \frac{\Delta K_1}{dt} \right| \right\rangle_t = \left\langle \left| \frac{K_1(t) - K_1(t - dt)}{dt} \right| \right\rangle_t, \quad (22)$$

where $K_1 = \frac{1}{2}\dot{x}_1^2$ is the kinetic energy of the first particle. Equation (22) is similar to the quantity $\langle \left| \frac{\Delta K}{dt} \right| \rangle_t$ of the left hand side of Eq. (25).

2.4 Set of initial conditions

We prepare the two systems in a systematic way to reside in a chaotic regime and be able to produce information. For example, for the SPO2 we follow Ref. [23] and consider $\beta = 1$ and $N = 14$ varying the energy and initial condition $\vec{X}(0)$ appropriately as following: For each fixed energy E of Hamiltonian (3), an initial condition $\vec{X}(0) = (\vec{x}(0), \dot{\vec{x}}(0))$ is chosen (where $\vec{x}(t) = (x_1(t), x_2(t), \dots, x_N(t))$ and $\dot{\vec{x}}(t) = (\dot{x}_1(t), \dot{x}_2(t), \dots, \dot{x}_N(t))$) so that it lies in the neighborhood of SPO2. By neighborhood we mean that we perturb the equations of motion by a controllable small perturbation (i.e. $\hat{x}(t) = \hat{x}(t) - 10^{-15}$) so that the perturbed initial condition $\vec{X}(0)$ will be at the same constant energy E of SPO2. Easily, we can fulfill this requirement by solving Eq. (3) for $\dot{x}(N)$ and then substitute it in the initial condition. A demonstration of the importance of this can be found in Sec. 3 where we present the relation between the largest Lyapunov exponent of the KP space and of the FPU Hamiltonian.

We thus end up with 14 nodes, each interacting with its nearest neighbours in a 1-dimensional lattice with fixed ends. In our example, SPO2 is destabilized at the energy $E_U \approx 0.117$ and restabilized again at $E_R \approx 47.059$ [23]. Thus, as E increases in (E_U, E_R) , SPO2 is unstable and gives rise initially to weakly and then to strongly chaotic behaviour in its neighborhood. For each E we numerically integrate the

corresponding initial condition $\vec{X}(0)$ and compute the Lyapunov exponents following Refs. [2, 7, 8] until they show a clear tendency to converge to a value. We subsequently record their values at the final integration time t_f . In our case, we have checked that this convergence happens at about $t_f = 2 \times 10^6$. We denote them as λ_i , $i = 1, \dots, N$ arranged in descending order. In terms of the numerical integration, we try to satisfy the condition that the relative energy error is kept between 10^{-6} and 10^{-13} . We follow a similar approach for the initial conditions we set in the neighborhood of SPO1 mode of FPU and OPM mode of BEC so that we can guarantee chaotic behavior with the increase of the energy of the system.

3 Results

3.1 Relation between largest Lyapunov exponent of the bi-dimensional KP space and of the Hamiltonian

The dynamics on the KP space is driven by the dynamics of the Hamiltonian system and we have no explicitly given equations of motion for the KP space. As we have already pointed out, we choose initial conditions $\vec{X}(0)$ on the same energy as the SPO2, and this implies that points $(K(\vec{X}_1(t)), P(\vec{X}_1(t)))$ and $(K(\vec{X}_2(t)), P(\vec{X}_2(t)))$ belong to the line $K(\vec{X}(t)) + P(\vec{X}(t)) = E$. The motion takes place on this 1-dimensional subspace and thus, there is only one Lyapunov exponent λ_1^{KP} that leads to $I_c^{KP} = \lambda_1^{KP}$.

In Fig. 1, one can see schematically the time evolution after one time step dt of a deviation vector (denoted as an arrow) along the direction of the Lyapunov exponent λ_1^{KP} defined for the dynamics on the line $K + P = E$. Here $\vec{X}_1(t)$ and $\vec{X}_2(t)$ are two trajectories in the phase space of Hamiltonian (3) on the same energy E as SPO2, started initially in its neighborhood and being infinitesimally close. Then, λ_1^{KP} is the rate of expansion of the deviation vector defined by the points $(K(\vec{X}_1(t)), P(\vec{X}_1(t)))$ and $(K(\vec{X}_2(t)), P(\vec{X}_2(t)))$. Here, δ and Δ denote the lengths of the initial and after one time step deviation vectors respectively.

λ_1^{KP} can be defined for infinitesimally close-by points on the 1-dimensional space of $K + P = E$ of Fig. 1 by keeping track of the evolution of their distance. In particular, for such points $(K(\vec{X}_1(t)), P(\vec{X}_1(t)))$

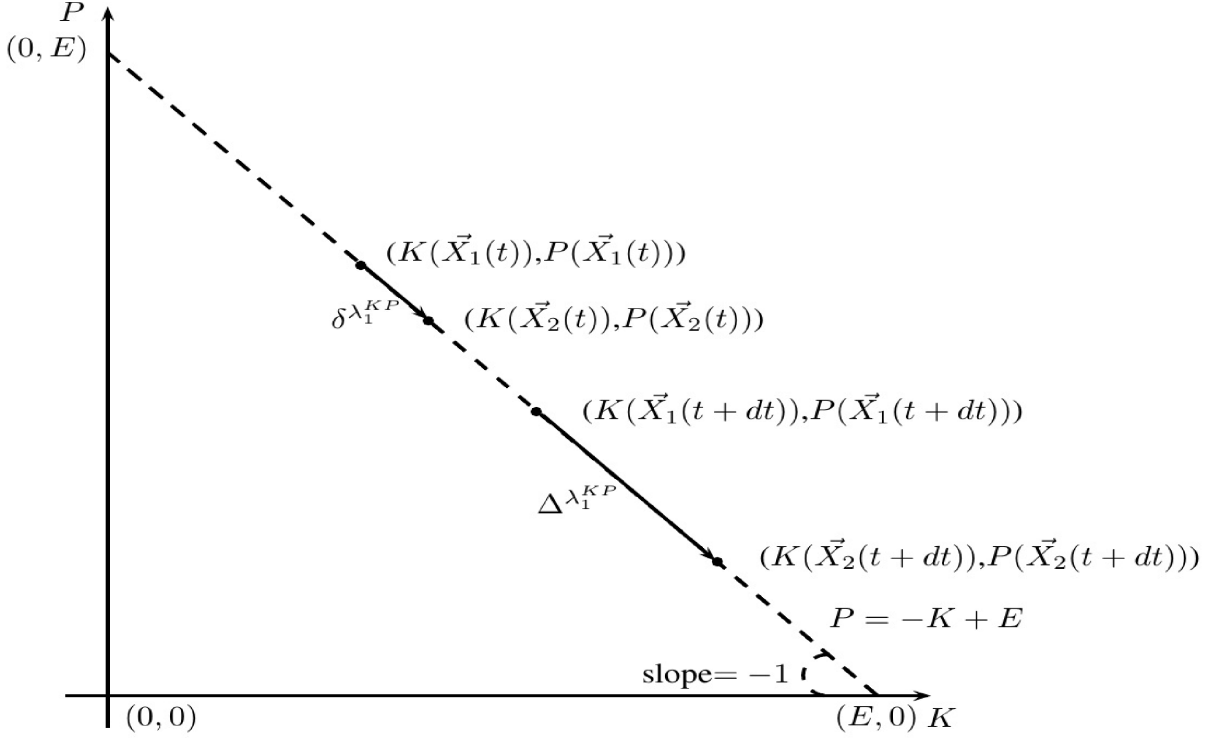


Figure 1. Schematic representation of the time evolution after one time step dt of two deviation vectors (arrows) corresponding to the direction along the Lyapunov exponent λ_1^{KP} on the 1-dimensional subspace $K + P = E$ on the KP space. $\vec{X}_1(t)$ and $\vec{X}_2(t)$ are two trajectories in the phase space of Hamiltonian (3) that drive the dynamics along this line. We denote with δ and Δ the lengths of the two deviation vectors initially and after one time step, respectively.

and $(K(\vec{X}_2(t)), P(\vec{X}_2(t)))$, their distance is given by:

$$\begin{aligned}
 \Delta K_X(t)^2 &= (K(\vec{X}_1(t)) - K(\vec{X}_2(t)))^2 + (P(\vec{X}_1(t)) - P(\vec{X}_2(t)))^2 = \\
 &= (K(\vec{X}_1(t)) - K(\vec{X}_2(t)))^2 + (E - K(\vec{X}_1(t)) - E + K(\vec{X}_2(t)))^2 = \\
 &= 2(K(\vec{X}_1(t)) - K(\vec{X}_2(t)))^2 \Rightarrow \\
 \Delta K_X(t) &= \sqrt{2}|K(\vec{X}_1(t)) - K(\vec{X}_2(t))|. \tag{23}
 \end{aligned}$$

Defining:

$$\lambda_1^{KP} = \lim_{t \rightarrow \infty} \frac{1}{t} \log \left(\frac{\Delta K(t)}{\Delta K(0)} \right) \text{ for } \Delta K(0) \rightarrow 0,$$

and combining it with Eq. (23) we obtain:

$$\lambda_1^{KP} = \lim_{t \rightarrow \infty} \frac{1}{t} \log \left(\frac{|K(\vec{X}_1(t)) - K(\vec{X}_2(t))|}{|K(\vec{X}_1(0)) - K(\vec{X}_2(0))|} \right). \quad (24)$$

We denote as λ_1 the largest Lyapunov exponent in the neighborhood of SPO2, and reside on numerical simulations to show in Fig. 2 that λ_1^{KP} is actually λ_1 . In the example of Fig. 2 we have set $E = 30$, resulting in the relation $K + P = 30$. However, we have checked that the above result is valid for all energies we considered in (E_u, E_r) . We observe that $|\lambda_1 - \lambda_1^{KP}|$ tends to zero in the course of time and that at some point starts to saturate at about 10^{-4} due to round off numerical errors. In other words, we have showed that the largest Lyapunov exponent of the 1-dimensional $K + P = E$ space is equal to the largest Lyapunov exponent λ_1 of Hamiltonian (3), i.e. $\lambda_1^{KP} = \lambda_1$.

To achieve this result, we integrated simultaneously two infinitesimally close trajectories $\vec{X}_1(t)$ and $\vec{X}_2(t)$ (e.g. at an initial distance of the order of 10^{-7}) on the same energy as SPO2 and consider thus that $\Delta K(0) \approx 10^{-7}$, and replace the limits in Eq. (24) by a finite time $t = 2 \times 10^6$, computing λ_1^{KP} as a time average [8], i.e. as finite size and finite time Lyapunov exponent. Since for chaotic trajectories, the distance between $\vec{X}_1(t)$ and $\vec{X}_2(t)$ quickly saturates, we periodically renormalize their separation without altering their relative orientation in phase space and then compute the new distance $|K(\vec{X}_1(t)) - K(\vec{X}_2(t))|$ setting $|K(\vec{X}_1(0)) - K(\vec{X}_2(0))| = |K(\vec{X}_1(t - dt)) - K(\vec{X}_2(t - dt))|$. To avoid any numerical overflows, we preferred to do this at every time step.

Note that $\lambda_1^{KP} = \lambda_1$ is not an unexpected result, since the largest Lyapunov exponent should be obtained in typical low-dimensional linear projections or embedding spaces [3, 32]. By typical here we mean bi-dimensional subspaces or projections that are not oriented along Lyapunov vectors. However, the KP space is a highly nonlinear projection still maintaining the largest positive Lyapunov exponent of the Hamiltonian as we have demonstrated. Every initial condition creates a trajectory with only one positive Lyapunov exponent in the KP subspace. Therefore, $I_c^{KP} = \lambda_1^{KP}$.

Concluding this part, we have demonstrated that the transfer of information from K to P is mediated by the largest Lyapunov exponent of the Hamiltonian. We finally obtain:

$$\text{MIR}^{KP} \leq I_c^{KP} = \lambda_1^{KP} = \lambda_1.$$

The last result implies that the upper bound I_c^{KP} for the MIR^{KP} between kinetic and potential energies

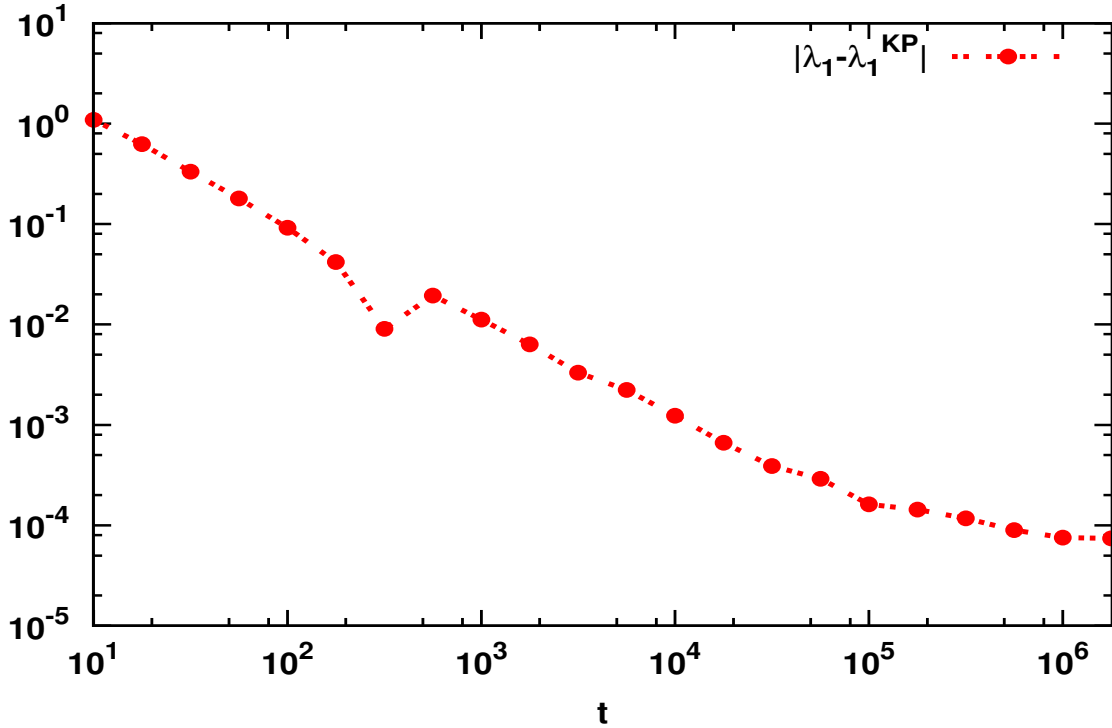


Figure 2. Plot of the absolute difference $|\lambda_1 - \lambda_1^{KP}|$ as a function of time for two trajectories $\vec{X}_1(t)$ and $\vec{X}_2(t)$ located initially in the neighborhood of SPO2 at the same energy E . Here, $E = 30$ is well inside the interval (E_u, E_T) . Note that both axes are logarithmic.

is equal to the largest Lyapunov exponent of the Hamiltonian and consequently, MIR^{KP} can not be bigger than this exponent.

3.2 Relation between production and transfer of information in the small energy regime

To start with, we present in a log-log plot in Fig. 3 the quantities I_c of Eq. (18) in red dashed line with points, H_{KS} of Eq. (1) in green dashed line with rectangles, $I_c^{KP} = \lambda_1$ in black solid line with lower triangles and $\langle |\frac{\Delta K}{dt}| \rangle_t$ of Eq. (21) in blue dashed line with upper triangles for the SPO2 case of the FPU system with parameters as defined in Subsec. 2.1. Here dt is the time step of the integration (i.e. $dt \ll 1$). The time derivative of the kinetic energy $\frac{dK}{dt}$ accounts for the rate of transfer from kinetic to potential energy. We see that all quantities follow the same morphology (i.e. share the same functional

form) as the energy of the initial condition $\vec{X}(0)$ is increased in the interval (E_U, E_T) . Moreover, H_{KS} is an upper bound of the upper bound I_c for the MIR between two groups formed each by 7 nodes. We will prove a related inequality in the Appendix.

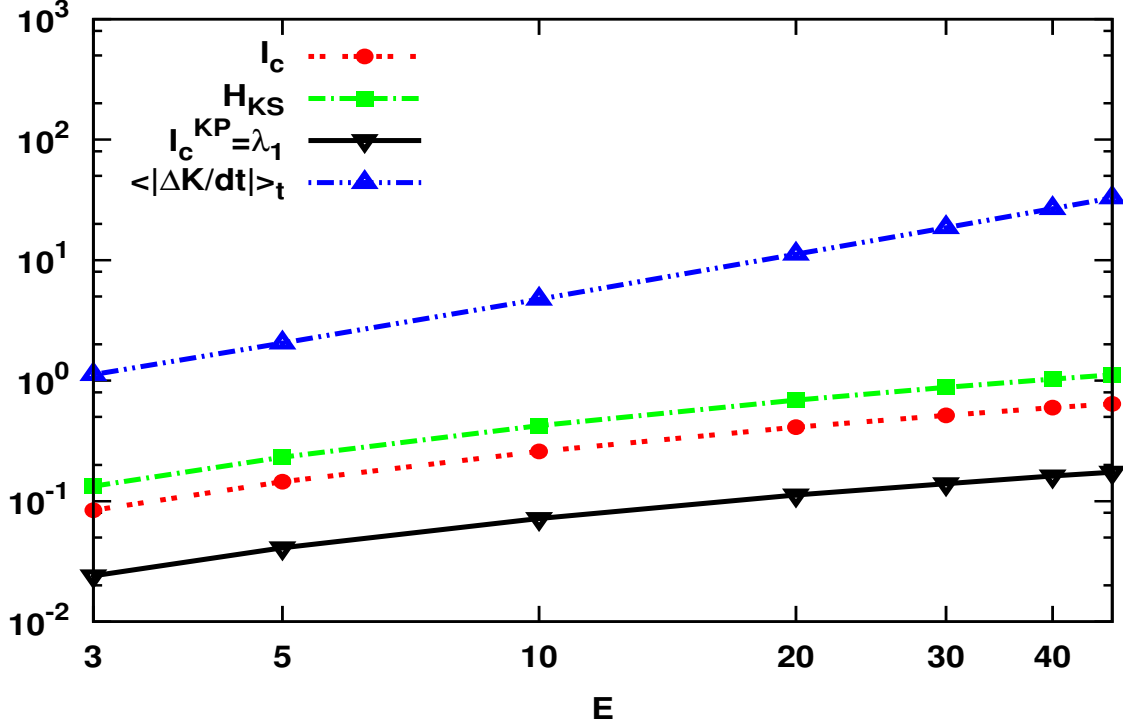


Figure 3. Plot of the quantities: I_c as defined by Eq. (18) in red dashed line with points, H_{KS} as defined by Eq. (1) in green dashed line with rectangles, I_c^{KP} as defined by Eq. (19) in black solid line with lower triangles and $\langle |\frac{\Delta K}{dt}| \rangle_t$ as defined by Eq. (21) in blue dashed line with upper triangles as a function of E for initial conditions $\vec{X}(0)$ located in the neighborhood of SPO2 of the FPU system. Note that both axes are logarithmic.

The approach we shall follow to relate $\langle |\frac{\Delta K}{dt}| \rangle_t$ with I_c^{KP} for the transfer of information between K and P is meaningful as long as the motion in the Hamiltonian phase space is chaotic (e.g. as long as $E \in (E_U, E_T)$). If the motion is periodic or quasi-periodic there is no exchange of information between the nodes (i.e. by knowing the position of a particular node one can predict the position and momenta of another one). Our results show that $\langle |\frac{\Delta K}{dt}| \rangle_t$ is related by a power-law to the largest Lyapunov exponent λ_1 of the Hamiltonian and to the upper bound I_c^{KP} for the transfer of information between kinetic and potential energies. Surprisingly, we have found that this is valid for sufficiently large enough subintervals,

i.e. for $E \in (E_u, E_r)$.

Here, we need to make use of only one neighboring initial condition $\vec{X}(0)$ of SPO2 and denote for simplicity by $K(t) \equiv K(\vec{X}(t))$. With the help of Eq. (21) and $\Delta K \equiv \Delta K(t) = K(t) - K(t - dt)$ we have found numerically that:

$$\left\langle \left| \frac{\Delta K}{dt} \right| \right\rangle_t \propto E^{b_2} \quad (25)$$

for the same energy interval that Eq. (20) applies where b_2 is a real positive constant. By substituting Eq. (20) in Eq. (25), we obtain:

$$\left\langle \left| \frac{\Delta K}{dt} \right| \right\rangle_t \propto \left(I_c^{KP} \right)^{\frac{b_2}{b_1}} = \left(\lambda_1^{KP} \right)^{\frac{b_2}{b_1}}, \quad (26)$$

where we have used $I_c^{KP} = \lambda_1$ (see Subsec. 3.1). It is straightforward to show that the same power-law (26) applies to $\left\langle \left| \frac{\Delta P}{dt} \right| \right\rangle_t$ due to Eqs. (14) and (16) respectively. We emphasize that $\left| \frac{\Delta K}{dt} \right|$ is a time-ratio that depends on time, and that $\left\langle \left| \frac{\Delta K}{dt} \right| \right\rangle_t$ and λ_1 are time invariant averages.

Fig. 4A shows in a log-log scale the quantity I_c of Eq. (18) in red dashed line with points and H_{KS} of Eq. (1) in green dashed line with rectangles. In panel B, we plot $I_c^{KP} = \lambda_1$ with red points and the power-law fitting:

$$\lambda_1 = a_1 E^{b_1} \quad (27)$$

with green line. The agreement is remarkable. In Fig. 4C we plot $\left\langle \left| \frac{\Delta K}{dt} \right| \right\rangle_t$ of Eq. (25) and fit with the power-law:

$$\left\langle \left| \frac{\Delta K}{dt} \right| \right\rangle_t = a_2 E^{b_2} \quad (28)$$

showed as green line. We find that $a_1 \approx 0.03$, $b_1 \approx 0.489$ and that $a_2 \approx 0.25$, $b_2 \approx 1.267$. In panel D of the same figure we plot $\left\langle \left| \frac{\Delta K}{dt} \right| \right\rangle_t$ with red points as a function of $I_c^{KP} = \lambda_1$ for values that correspond to the same energy interval of panels A, B and C. The power-law fitting:

$$\left\langle \left| \frac{\Delta K}{dt} \right| \right\rangle_t \approx a_3 (\lambda_1)^{b_3} \quad (29)$$

plotted in green dashed line gives $a_3 \approx 3077.79$ and $b_3 \approx 2.60$ which is in good agreement with the value

of $b_2/b_1 \approx 2.591$. The above arguments directly imply that:

$$\left\langle \left| \frac{\Delta K}{dt} \right| \right\rangle_t \propto \left(I_c^{KP} \right)^{\frac{b_2}{b_1}} = \left(\frac{2H_{\text{KS}}}{N} \right)^{\frac{b_2}{b_1}}, \quad (30)$$

where the proportionality constant $a_3 = a_2 \left(\frac{1}{a_1} \right)^{\frac{b_2}{b_1}}$ and $b_3 = b_2/b_1$. To arrive at Eq. (30) we have used $I_c^{KP} = \lambda_1$ of Subsec. 3.1 and Eq. (39) presented in the Appendix. Equation (30) relates the production λ_1 and transfer of information I_c^{KP} in the KP space with $\left\langle \left| \frac{\Delta K}{dt} \right| \right\rangle_t$ and H_{KS} . Therefore, the larger the transfer of energy is between the kinetic and potential energy, the larger is the upper bound for the MIR between the kinetic and potential energies and the larger the KS entropy of the system will be. In other words, exchange of information between K and P implies exchange of energy, and vice-versa. However, a relatively small increment of energy transfer produces a larger relative increase of the information transferred since $b_3 > 1$.

In the Appendix we prove another important result which is the inequality:

$$I_c^{KP} < I_c < H_{\text{KS}}, \quad (31)$$

and thus justify the result presented in Fig. 3.

3.3 Generalization of our study

Here, we extend our study and present the generalization of our predicted upper bounds for the MIR and the connection with the transfer of energy of the previous section by considering higher energy intervals with initial conditions set in different parts of the phase space of two Hamiltonian systems: the FPU (3) and BEC (10).

We will show that if one considers a much larger energy interval for these systems with initial conditions set in different parts of their phase spaces, then Eqs. (27), (28) and (29) can be generalized, as:

$$I_c^{\text{BS}} = a_4 + b_4 E^{c_4}, \quad a_4, b_4, c_4 \in \mathbb{R}, \quad (32)$$

$$\left\langle \left| \frac{\Delta K}{dt} \right| \right\rangle_t = a_5 + b_5 (c_5 + E)^{d_5}, \quad a_5, b_5, c_5, d_5 \in \mathbb{R}. \quad (33)$$

We prefer to call Eqs. (32) and (33) as generalized power-law functions. Here, BS stands for the bi-

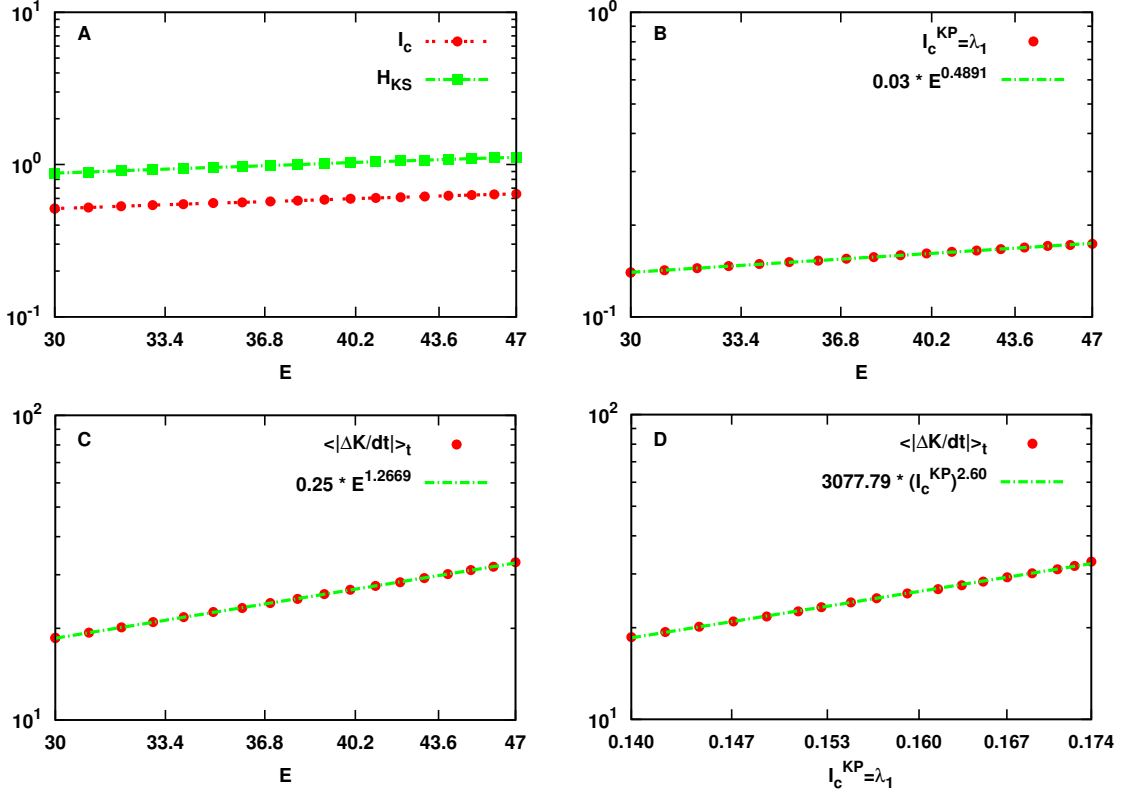


Figure 4. Panel A: Plot of quantities: I_c of Eq. (18) in red dashed line with points and H_{KS} of Eq. (1) in green dashed line with rectangles. Panel B: Plot of quantities $I_c^{KP} = \lambda_1$ with red points with the power-law fitting of Eq. (27) in green line. Panel C: Plot of $\langle |\frac{\Delta K}{dt}| \rangle_t$ with red points with the power-law fitting of Eq. (29) in green line. Panel D: Power-law dependence of $\langle |\frac{\Delta K}{dt}| \rangle_t$ to $I_c^{KP} = \lambda_1$ in red points, in the interval $(0.140, 0.174)$ that corresponds to the energy interval $[30, 47]$ of panels A, B and C and of the power-law fitting of Eq. (29) in green dashed line. Note that all axes are logarithmic.

dimensional space of observation. In the case of the FPU system (3) we consider as a bi-dimensional space the KP space while for the BEC system (10) we consider the observation space constructed by observing the pair of variables x_1 and x_N , that is by the position of the first and last particle. In Sec. 4, where we study an “experimental” setup of a 1-dimensional communication channel based on the FPU system, we will use this particular observation space as well.

By eliminating E from both Eqs. (32) and (33), one arrives at the relation between transfer of energy per unit of time (i.e. $\langle |\frac{\Delta K}{dt}| \rangle_t$) and upper bound of information transmitted in the bi-dimensional space

BS (i.e. I_c^{BS}):

$$f(I_c^{\text{BS}}) = \left\langle \left| \frac{\Delta K}{dt} \right| \right\rangle_t = a_6 + b_6 \left[c_6 + \left(\frac{d_6 + I_c^{\text{BS}}}{e_6} \right)^{f_6} \right]^{g_6}, \quad a_6, b_6, c_6, d_6, e_6, f_6, g_6 \in \mathbb{R}. \quad (34)$$

Parameters $a_i, b_i, c_i, d_i, e_i, f_i, g_i$ can be determined by performing a non-linear fitting of the numerical data by the functions (32), (33) and (34). We have used Matlab to perform these fittings.

3.3.1 FPU SPO2

In the case of the SPO2 studied in Subsec. 3.2, the fit of Fig. 4 was performed in the energy interval [30, 47]. Here we generalize Eqs. (27), (28) and (29) in the larger energy interval [3, 47] for which the dynamics around SPO2 is chaotic as indicated by the Lyapunov exponents. This allows the creation and transfer of information and energy. We have used the same parameters and setup (e.g. 14 particles) to allow for a direct comparison between Figs. 4 and 5.

By doing a similar analysis as in Subsec. 3.2, we present in Fig. 5 the plots of all relevant quantities for the larger energy interval. By fitting the new data with the generalized power-laws of Eqs. (32), (33) and (34) we have: $a_4 \approx -0.07$, $b_4 \approx 0.07$, $c_4 \approx 0.34$ for Eq. (32), $a_5 \approx -1.16$, $b_5 \approx 0.18$, $c_5 \approx 3.64$, $d_5 \approx 1.34$ for Eq.(33) and finally: $a_6 \approx -14.83$, $b_6 \approx 2.27 \times 10^{-15}$, $c_6 \approx 32.41$, $d_6 \approx 0.01$, $e_6 \approx 0.1$, $f_6 \approx 1.97$ and $g_6 \approx 10.47$ for Eq. (34).

3.3.2 FPU SPO1

Here we extend our study to a another part of the phase space of the FPU Hamiltonian with initial conditions set in the neighborhood of the periodic orbit SPO1 (see Eq. (4) of Subsec. 2.1). We have chosen this particular part of the phase space as SPO1 does not restabilize at some bigger energy as it happens with SPO2 and thus allows to reach as high energies as desired. We will show that the same generalized power-laws of Eqs. (32), (33) and (34) can still be used to fit the data of the upper bounds for MIR such as I_c , H_{KS} and I_c^{KP} . In more details, for Eq. (32) we have: $a_4 \approx -0.18$, $b_4 \approx 0.15$, $c_4 \approx 0.23$, for Eq.(33) we have: $a_5 \approx -0.99$, $b_5 \approx 0.26$, $c_5 \approx 0$, $d_5 \approx 1.25$ and finally, for Eq. (34) we have: $a_6 \approx -14.33$, $b_6 \approx 2.91$, $c_6 \approx 1.68$, $d_6 \approx -0.08$, $e_6 \approx 0.17$, $f_6 \approx 1.39$ and $g_6 \approx 3.62$.

In Fig. 6 we present the corresponding plots and fits for the energy interval [3, 10⁴] considering 15 particles and $\beta = 1$. Following Ref. [23], for these values we know that the dynamics around SPO1 is

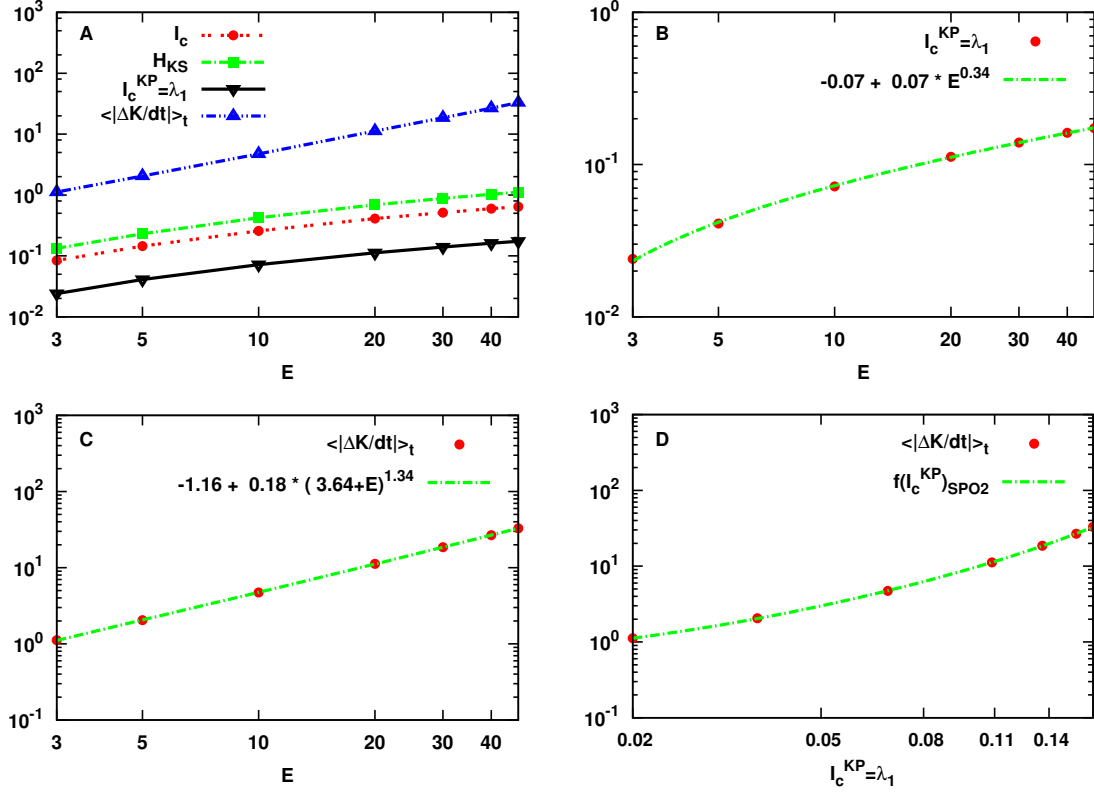


Figure 5. Panel A: Plot of quantities: I_c as defined by Eq. (18) in red dashed line with points, H_{KS} as defined by Eq. (1) in green dashed line with rectangles, I_c^{KP} as defined by Eq. (19) in black solid line with lower triangles and $\langle |\frac{\Delta K}{dt}| \rangle_t$ as defined by Eq. (21) in blue dashed line with upper triangles as a function of E for initial conditions $\vec{X}(0)$ located in the neighborhood of SPO2 of the FPU system. Note that both axes are logarithmic. Panel B: Plot of $I_c^{KP} = \lambda_1$ with red points with the power-law fitting of Eq. (32) in green line. Panel C: Plot of $\langle |\frac{\Delta K}{dt}| \rangle_t$ with red points with the power-law fitting of Eq. (33) in green line. Panel D: Power-law dependence of $\langle |\frac{\Delta K}{dt}| \rangle_t$ to $I_c^{KP} = \lambda_1$ in red points, in the interval $(0.02, 0.174)$ that corresponds to the energy interval $[3, 47]$ of panels A, B and C and of the power-law fitting of Eq. (33) in green dashed line. Note that all axes are logarithmic.

chaotic and thus allows the production and exchange of energy and information in the FPU chain.

3.3.3 BEC OPM

Next, we proceed and study the same problem for a different system, namely the BEC Hamiltonian given in Eq. (10). We have chosen this system as it allows us to study the relation between transfer and exchange of energy and information in a different Hamiltonian system than the FPU. Furthermore, because it is not written in the form $H = K + P$ as the FPU does (compare Eqs. (3) and (10)). It will

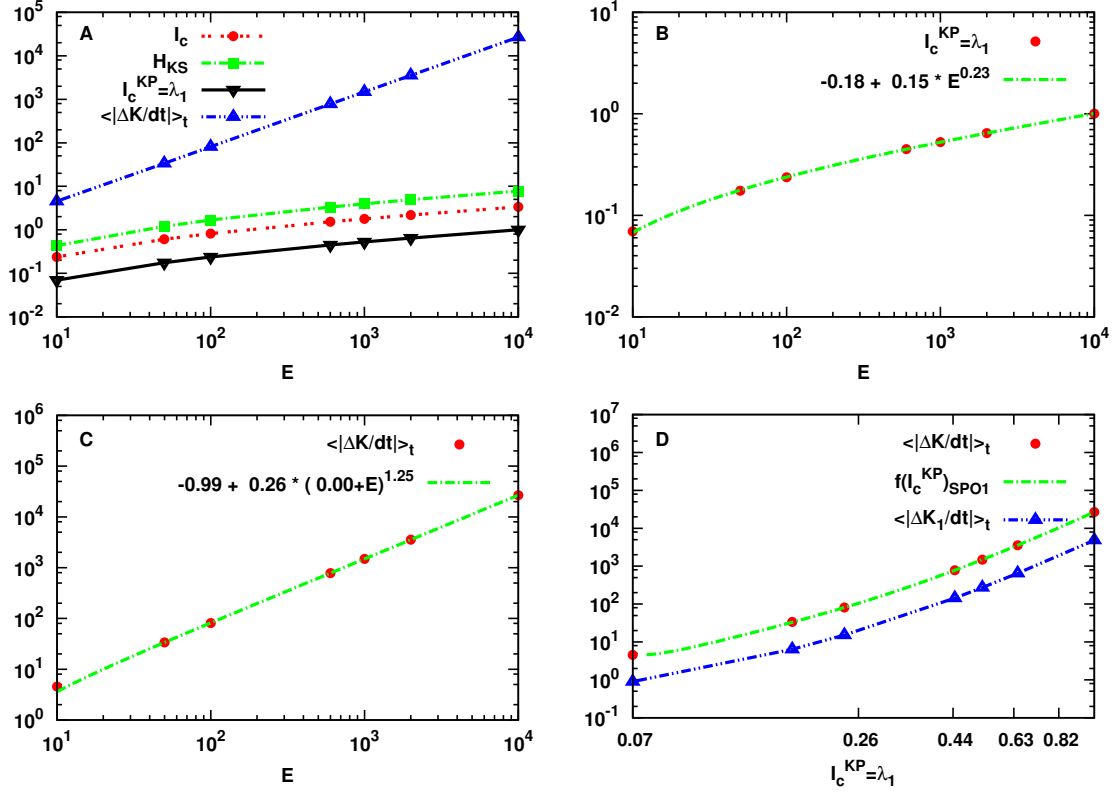


Figure 6. Panel A: Plot of quantities: I_c as defined by Eq. (18) in red dashed line with points, H_{KS} as defined by Eq. (1) in green dashed line with rectangles, I_c^{KP} as defined by Eq. (19) in black solid line with lower triangles and $\langle |\frac{\Delta K}{dt}| \rangle_t$ as defined by Eq. (21) in blue dashed line with upper triangles as a function of E for initial conditions $\vec{X}(0)$ located in the neighborhood of SPO1 of the FPU system. Note that both axes are logarithmic. Panel B: Plot of $I_c^{KP} = \lambda_1$ with red points with the power-law fitting of Eq. (32) in green line. Panel C: Plot of $\langle |\frac{\Delta K}{dt}| \rangle_t$ with red points with the power-law fitting of Eq. (33) in green line. Panel D: Power-law dependence of $\langle |\frac{\Delta K}{dt}| \rangle_t$ to $I_c^{KP} = \lambda_1$ in red points, in the interval $(0.07, 1)$ that corresponds to the energy interval $[10, 10^4]$ of panels A, B and C and of the power-law fitting of Eq. (33) in green dashed line. Note that all axes are logarithmic.

thus permit us to demonstrate the validity of the upper bounds for the MIR and the connection between the exchange of energy and information in different observation spaces.

In particular, we consider here a small version of the system with $N = 6$ degrees of freedom (particles) with initial conditions set in the neighborhood of the OPM periodic orbit given in Eq. (13) with periodic boundary conditions (see Eq. (12)). In Fig. 7, we show the results of a similar study as we did in the cases of SPO1, SPO2 of the FPU system, for the energy interval $(3.94, 1037.56)$ for which we have been able to study numerically in terms of the preservation of the accuracy of the computed energy. For this

energy interval we know that the dynamics is chaotic (see Ref. [24]). Since, as we have already pointed out, BEC is not given by the sum of the kinetic and potential energy, we adopt a different strategy and reside on the calculation of the similar quantity $\langle |\frac{\Delta K_1}{dt}| \rangle_t$ based on the kinetic energy of the first particle x_1 (see Eq. (22)). However, the kinetic energy of any other particle can be used as well. By fitting the data with the generalized power-laws of Eqs. (32), (33) and (34) we have: $a_4 \approx -0.33$, $b_4 \approx 0.28$, $c_4 \approx 0.17$ for Eq. (32), $a_5 \approx -9.1$, $b_5 \approx 0.11$, $c_5 \approx 32.41$, $d_5 \approx 1.26$ for Eq.(33) and finally: $a_6 \approx -9.1$, $b_6 \approx 0.11$, $c_6 \approx 32.41$, $d_6 \approx 0.36$, $e_6 \approx 0.31$, $f_6 \approx 6.29$ and $g_6 \approx 1.27$ for Eq. (34).

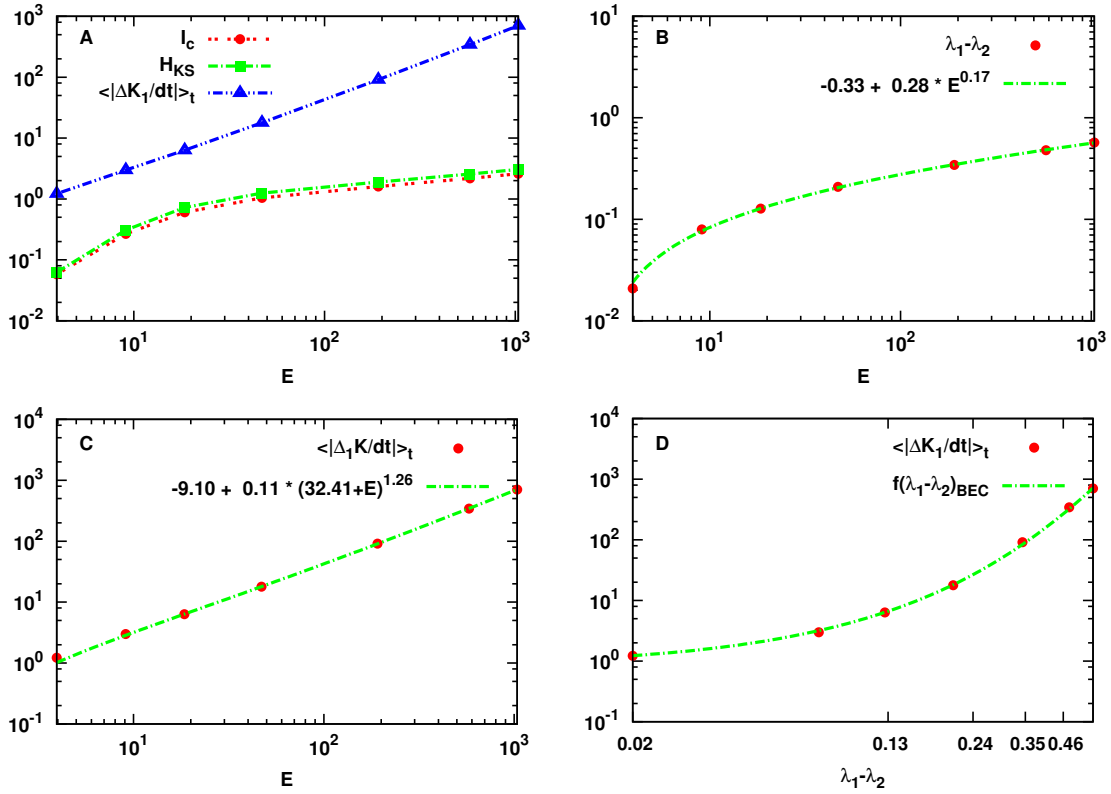


Figure 7. Panel A: Plot of quantities: I_c as defined by Eq. (18) in red dashed line with points, H_{KS} as defined by Eq. (1) in green dashed line with rectangles, I_c^{KP} as defined by Eq. (19) in black solid line with lower triangles and $\langle |\frac{\Delta K_1}{dt}| \rangle_t$ as defined by Eq. (22) in blue dashed line with upper triangles as a function of E for initial conditions $\vec{X}(0)$ located in the neighborhood of the OPM of the BEC Hamiltonian. Note that both axes are logarithmic. Panel B: Plot of $(\lambda_1 - \lambda_2)$ with red points with the power-law fitting of Eq. (32) in green line. Panel C: Plot of $\langle |\frac{\Delta K_1}{dt}| \rangle_t$ with red points with the power-law fitting of Eq. (33) in green line. Panel D: Power-law dependence of $\langle |\frac{\Delta K_1}{dt}| \rangle_t$ to $(\lambda_1 - \lambda_2)$ in red points, in the interval $(0.02, 0.57)$ that corresponds to the energy interval $(3.94, 1037.56)$ of panels A, B and C and of the power-law fitting of Eq. (33) in green dashed line. Note that all axes are logarithmic.

4 Hamiltonian Communication System

In this section we present an “experimental” implementation of a 1-dimensional communication channel based on the FPU Hamiltonian system of Eq. (3), and show the relation between our proposed upper bounds for the MIR with the actual MIR measured for the exchange of information between the first and last particle of the channel.

In more details, we consider the FPU chain of N oscillators as a 1-dimensional communication channel where information and energy flow from one end to the other, i.e. from the first particle x_1 to the last one x_N and vice versa. To extend the applicability of our theoretical results obtained in the previous sections for different cases of chaotic dynamics, we will use the dynamics around SPO1 and SPO2 and consider as a bi-dimensional observation space the one constructed by the evolution of the pair of position variables x_1, x_N of the first and last particle of the FPU chain of Eq. (3). The computation of the actual MIR value between the two observation nodes x_1 and x_N was based on the theory presented in Ref. [10]. Here, we consider 15 oscillators (degrees of freedom) for the SPO1 and 14 for the SPO2.

In panel A of Fig. 8 we show the results of our study for the SPO2 case. We have plotted in red dashed line with points the quantity I_c of Eq. (18), H_{KS} as defined by Eq. (1) in green dashed line with rectangles, I_c^{KP} of Eq. (19) in black solid line with lower triangles and $MIR_{1,14}$ in blue dashed line with upper triangles as a function of the energy E . Here, $MIR_{1,14}$ stands for the actual mutual information rate measured for the exchange of information between x_1 and x_{14} . From our theoretical results derived in the previous sections we expect that $MIR_{1,14}$ should be smaller or equal than I_c^{KP} . This is indeed what one observes as the $MIR_{1,14}$ curve is smaller than the previously mentioned upper bound and more importantly, it follows the same morphology (functional form) as I_c , H_{KS} and I_c^{KP} . We have performed the same analysis for the SPO1 case as well showed in panel B of the same figure and arrive again at the same conclusions, i.e. $MIR_{1,15}$ lies below I_c^{KP} as expected by our study and follows the same morphology as the upper bounds I_c , H_{KS} and I_c^{KP} . In this case, $MIR_{1,15}$ denotes the actual mutual information rate measured for the exchange of information between x_1 and x_{15} .

5 Discussion

In this paper we have studied the relation among the transfer of energy from kinetic (K) to potential (P) energies, the transfer of information between these two quantities and between different particles,

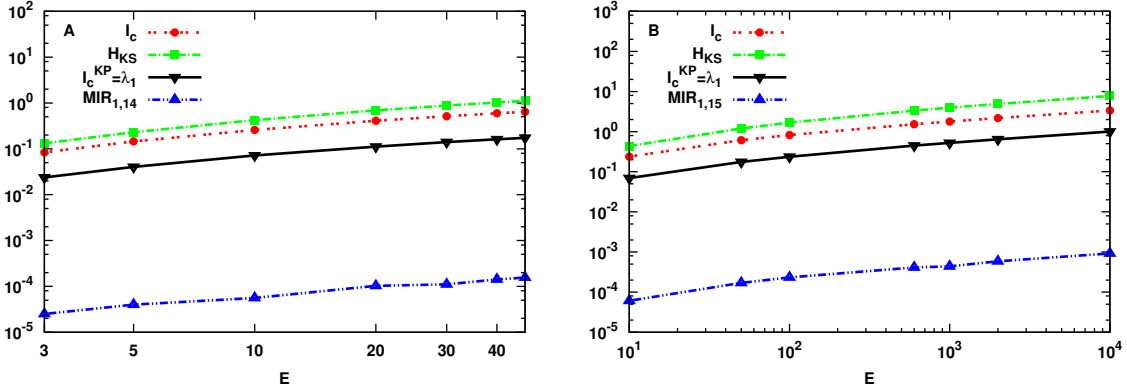


Figure 8. Panel A: Plot of the quantity I_c as defined by Eq. (18) in red dashed line with points, H_{KS} as defined by Eq. (1) in green dashed line with rectangles, I_c^{KP} as defined by Eq. (19) in black solid line with lower triangles and $\text{MIR}_{1,14}$ in blue dashed line with upper triangles as a function of E for initial conditions $\vec{X}(0)$ set in the neighborhood of SPO2. Panel B: Same as in panel A for initial conditions set in the neighborhood of SPO1. Note that all axes are logarithmic.

the production of information, and Lyapunov exponents in Hamiltonian systems.

Our first result is that the largest Lyapunov exponent of the bi-dimensional space of the kinetic and potential energy is equal to the maximal Lyapunov exponent of the Hamiltonian in the case it is given by the sum of the kinetic and potential energy. Consequently, we were able to show that the upper bound for the MIR in the KP subspace is given by the largest Lyapunov exponent of the Hamiltonian (λ_1). This implies that the more information the Hamiltonian system produces (λ_1), the more information can be exchanged between K and P .

The second important result we have found is a power-law relation between the rate of transfer from kinetic to potential energy, the largest Lyapunov exponent of the Hamiltonian, and the Kolmogorov-Sinai entropy of the Hamiltonian. The more chaotic and the more information the Hamiltonian system produces (λ_1 and H_{KS}) respectively, the larger is the time average of the absolute value of energy transferred between K and P per unit of time (i.e. $\langle |\frac{\Delta K}{dt}| \rangle_t$).

The other important result is the proof of the inequality $I_c^{KP} < I_c < H_{\text{KS}}$ in the Appendix. It implies that, when one observes a Hamiltonian system through its kinetic and potential energies (thus obtaining I_c^{KP}), one measures less information about the Hamiltonian system than when observing half of its variables (thus obtaining I_c) or all of its variables (thus obtaining H_{KS}).

Finally, we have proposed an “experimental” implementation of a 1-dimensional communication chan-

nel based on a Hamiltonian system, and have calculated the actual rate with which information is exchanged between the first and last particle of the channel and compared that with the upper bounds we have proposed. As expected from our theoretical analysis, in all cases we have studied the actual MIR values were found to be smaller than our proposed upper bounds of MIR.

It is challenging to sketch here a possible connection between our results and the free energy F , entropy S , temperature T and Hamiltonian energy E in the thermodynamic limit, i.e. when E and N grow indefinitely while their ratio E/N remains constant. According to the definition attributed to Helmholtz, F is equal to the internal energy of the system U minus the product of the (absolute) temperature T multiplied by S , i.e. $F = U - TS$. T is an important macroscopic quantity since its definition goes back to the early days of thermodynamics. Maxwell had realized that when the Hamiltonian has the special form:

$$H(x, \dot{x}) = \frac{1}{2}\dot{x}^2 + P(x, \dots),$$

(as is the case of the FPU system we have studied in this work) the canonical ensemble average of \dot{x}^2 is the temperature T of the system. Thus, if one assumes ergodicity and equivalence of ensembles of initial conditions, it suffices to measure the time average of \dot{x}^2 during the evolution of the system in order to compute T (see for example Ref. [33]). Then, U in this context is the fixed energy of the Hamiltonian (e.g. FPU) $E(= K + P)$ and S can be calculated by the KS entropy H_{KS} as $S = \alpha H_{\text{KS}}$, where α has the unit of time, since KS entropy is simply Shannon's entropy (equivalent to Gibb's entropy) per unit of time. Therefore, one can have:

$$\begin{aligned} F &= E - T\alpha H_{\text{KS}} \Rightarrow \\ F &= K + P - T\alpha H_{\text{KS}}, \end{aligned} \tag{35}$$

and by solving Eq. (35) to obtain:

$$H_{\text{KS}} = \frac{K + P - F}{\alpha T}. \tag{36}$$

If Eq. (30) remains still valid in the thermodynamic limit, then by substituting Eq. (36) in the right hand side of Eq. (30) one has:

$$\left\langle \left| \frac{\Delta K}{dt} \right| \right\rangle_t \propto \left(I_c^{KP} \right)^{\frac{b_2}{b_1}} = (\lambda_1)^{\frac{b_2}{b_1}} = \left(2 \frac{K + P - F}{\alpha TN} \right)^{\frac{b_2}{b_1}}, \tag{37}$$

which relates the rate of transfer from kinetic to potential energy and the largest Lyapunov exponent of the Hamiltonian with the free energy and temperature of the system. This provides a direct relation between the results of this paper and important quantities of thermodynamics and Statistical Mechanics as long as the same conditions required for the derivation of the main results of our paper hold for Eq. (37) as well. Equation (37) implies that the larger the gap between the energy of the Hamiltonian and the available energy to do work (the free energy) the smaller the transfer of energy and information from K to P is.

In a series of papers [20, 34–36], the authors discuss about technological applications of the transfer of energy and information in communication, interference and graphical networks and show how one can reuse part of the energy for successive communication tasks. These ideas are based on results from physics showing that any system that exchanges information via the transfer of given physical resources such as radio waves, particles, etc., can reuse part of the received resources. If chaotic Hamiltonian systems could be used to create a communication system such that energy of the transmitting signal could be reused to transmit more information, from Eq. (37) it is clear that F must be different than zero implying that less information can be transmitted.

We believe that our work provides a viable pathway to establish similar relations between production and transfer of energy and information in other Hamiltonian systems for which the Lyapunov exponents have different dependences with the increase of the energy of the system as compared to those we have found here. Moreover, the choice of the bi-dimensional observation space is not restrictive and a plausible one can be constructed by the position coordinates of any two particles of the system. Of course, in these cases it is expected that our power-law relations will be replaced by new ones reflecting the different properties of the systems.

Appendix

Here, we prove the other main result of this paper which is the inequality:

$$I_c^{KP} < I_c < H_{KS} \quad (38)$$

and thus explain the result of Fig. 3. In Ref. [31], the authors discuss about the existence of the spectrum of the Lyapunov exponents in the thermodynamic limit and investigate numerically this existence in the FPU- β model given herein by Eq. (3). They show that the shape of the Lyapunov spectrum for energy densities $\epsilon = E/N$ well above the equipartition threshold allows someone to express H_{KS} in terms of the largest Lyapunov exponent λ_1 only:

$$H_{\text{KS}} = \int_0^{\lambda_1} \lambda CN d\lambda = \frac{N}{2} \lambda_1, \quad (39)$$

where $C = 1/\lambda_1$.

By applying the above ideas in our case for $E \in (E_{\text{u}}, E_{\text{r}})$ and using Eq. (39) we have:

$$\begin{aligned} H_{\text{KS}} &= \int_0^{\lambda_1} \lambda CN d\lambda \Rightarrow \\ H_{\text{KS}} &= \int_0^{\lambda_{N/2}} \lambda CN d\lambda + \int_{\lambda_{N/2}}^{\lambda_1} \lambda CN d\lambda \Rightarrow \\ H_{\text{KS}} &= \frac{N}{2\lambda_1} (\lambda^2)_0^{\lambda_{N/2}} + \tilde{H} \Rightarrow \\ \tilde{H} &= H_{\text{KS}} - \frac{N}{2\lambda_1} (\lambda_{N/2})^2, \end{aligned} \quad (41)$$

where we have used $C = 1/\lambda_1$ and $\tilde{H} = \int_{\lambda_{N/2}}^{\lambda_1} \lambda CN d\lambda$. Term $\lambda_{N/2}$ is the $(N/2)$ th positive Lyapunov exponent of Hamiltonian (3) when sorting them in descending order (i.e. $\lambda_1 > \lambda_2 > \dots > \lambda_{N/2} > \dots > \lambda_N = 0$). It comes from the fact that in Eq. (40) we integrate over all positive Lyapunov exponents and that we want to relate H_{KS} with \tilde{H} of Eq. (18) which is defined as the sum over the first $N/2$ positive Lyapunov exponents when they are sorted in descending order.

By substituting Eq. (41) in Eq. (18) we have:

$$\begin{aligned} I_c &= 2\tilde{H} - H_{\text{KS}} \Rightarrow \\ I_c &= H_{\text{KS}} - \frac{N}{\lambda_1} (\lambda_{N/2})^2, \end{aligned} \quad (42)$$

and so we obtain:

$$I_c < H_{\text{KS}} \quad (43)$$

which is the right hand side inequality of Eq. (38).

By combining Eqs. (39), (42) and setting $I_c^{KP} = \lambda_1$, we obtain:

$$\begin{aligned} I_c &= \frac{N}{2} \lambda_1 - \frac{N}{\lambda_1} (\lambda_{N/2})^2 \Rightarrow \\ I_c &= \frac{N}{2} I_c^{KP} - \frac{N}{I_c^{KP}} (\lambda_{N/2})^2. \end{aligned} \quad (44)$$

The last equation links the upper bound of information transfer in the phase space of the Hamiltonian with the upper bound of the information that can be transferred in the KP space. Moreover, an important consequence of Eq. (42) is that $I_c = H_{\text{KS}}$ when $\lambda_{N/2} = 0$ implying that this can happen when there are at least $N/2$ integrals of motion and leading to the conclusion that it should be $\lambda_{N/2} = \lambda_{(N/2)+1} = \dots = \lambda_N = 0$. However, this is not happening in our case since all Lyapunov exponents are positive but the last one $\lambda_N = 0$ as the Hamiltonian is an integral of the motion.

Next, we prove the left hand side inequality of Eq. (38):

$$I_c^{KP} < I_c. \quad (45)$$

To do so, let us suppose that:

$$I_c - I_c^{KP} = 0 \quad (46)$$

and check under which assumptions for I_c^{KP} Eq. (45) holds. For this, we substitute Eq. (44) for I_c into Eq. (46) and have:

$$\left(\frac{N-2}{2}\right) (I_c^{KP})^2 - N (\lambda_{N/2})^2 = 0. \quad (47)$$

The last equation is a second degree polynomial with respect to I_c^{KP} . Its determinant is given by:

$$\mathcal{D} = 2N(N-2)(\lambda_{N/2})^2,$$

which is positive for $N > 2$ and thus, the two discrete real roots are:

$$\begin{aligned} I_c^{KP} &= \frac{\lambda_{N/2} \sqrt{2N(N-2)}}{N-2} > 0 \text{ and} \\ I_c^{KP} &= -\frac{\lambda_{N/2} \sqrt{2N(N-2)}}{N-2} < 0. \end{aligned} \quad (48)$$

By theory, we know that Eq. (47) is positive and thus inequality in Eq. (45) is true when $I_c^{KP} > \frac{\lambda_{N/2}\sqrt{2N(N-2)}}{N-2}$ since the term $\frac{N-2}{2}$ of I_c^{KP} is positive for $N > 2$.

The second root is not physically possible to exist since it would imply that $I_c^{KP} < 0$ for $N > 3$ contradicting to the fact that I_c^{KP} is positively defined. Thus, Eq. (46) is positive when $I_c^{KP} > \frac{\lambda_{N/2}\sqrt{2N(N-2)}}{N-2}$, which is always true, since $\lambda_{N/2} \ll 1$ and:

$$\lim_{N \rightarrow \infty} \frac{\sqrt{2N(N-2)}}{N-2} = \sqrt{2}.$$

Thus, we have proved that:

$$I_c^{KP} < I_c. \quad (49)$$

Combining Eqs. (43) and (49), we obtain:

$$I_c^{KP} < I_c < H_{\text{KS}}. \quad (50)$$

The way I_c is defined (see Eq. (18)) implies that $I_c < H_{\text{KS}}$ since $\tilde{H} < H_{\text{KS}}$. In panel A of Fig. 3 we can check that indeed inequality (50) is fulfilled.

Finally, it worths mentioning that according to Eq. (48) it is possible to have:

$$I_c^{KP} = I_c$$

that is, the upper bounds of information transfer in the bi-dimensional subspace and in the Hamiltonian to be equal when it happens that:

$$I_c^{KP} = \frac{\lambda_{N/2}\sqrt{2N(N-2)}}{N-2} = \sqrt{2}\lambda_{N/2}.$$

The last equation provides an alternative estimation of I_c^{KP} valid when:

$$I_c^{KP} = \lambda_1 = \sqrt{2}\lambda_{N/2}.$$

Acknowledgments

Ch. A. would like to dedicate this paper to his recently born nephew, sharing both a common period of being “in preparation”. The authors were partially supported by the “EPSRC EP/I032606/1” grant.

References

1. Shannon CE (1948) A mathematical theory of communication. *The Bell System Technical Journal* 27: 379.
2. Skokos C (2010) The Lyapunov characteristic exponents and their computation. *Lecture Notes in Physics* 790: 63-135.
3. Eckmann JP, Ruelle D (1985) Ergodic theory of chaos and strange attractors. *Rev Mod Phys* 57: 617-656.
4. Bountis T, Skokos H (2012) *Complex Hamiltonian Dynamics*. Springer-Verlag Berlin Heidelberg.
5. Pesin YB (1976) Invariant manifold families which correspond to nonvanishing characteristic exponents. *Izv Akad Nauk SSSR Ser Mat* 40: 1332.
6. Pesin YB (1977) Lyapunov characteristic exponents and smooth ergodic theory. *Uspekhi Matematicheskikh Nauk* 32: 196.
7. Benettin G, Galgani L, Giorgilli A, Strelcyn JM (1980) Lyapunov characteristic exponents for smooth dynamical systems and for Hamiltonian systems: A method for computing all of them. Part 1: Theory. *Meccanica* 15: 9-20.
8. Benettin G, Galgani L, Giorgilli A, Strelcyn JM (1980) Lyapunov characteristic exponents for smooth dynamical systems and for Hamiltonian systems: A method for computing all of them. Part 2: Numerical application. *Meccanica* 15: 21-30.
9. Ruelle D (1978) An inequality for the entropy of differentiable maps. *Bol Soc Bras Mat* 9: 83.
10. Baptista MS, Rubinger RM, Viana ER, Sartorelli JC, Parlitz U, et al. (2012) Mutual information rate and bounds for it. *PLoS One* 7: 10:e46745.

11. Machiori MA, Fariello R, de Aguiar MAM (2012) Energy transfer dynamics and thermalization of two oscillators interacting via chaos. *Phys Rev E* 85: 041119.
12. Mandal D, T QH, Jarzynski C (2013) Maxwell's refrigerator: An exactly solvable model. *Phys Rev Lett* 111: 030602.
13. Baptista MS, Kurths J (2005) Chaotic channel. *Phys Rev E* 72: 045202.
14. Baptista MS, Kurths J (2008) Transmission of information in active networks. *Phys Rev E* 77: 026205.
15. Baptista MS, de Carvalho JX, Hussein MS (2008) Finding quasi-optimal network topologies for information transmission in active networks. *PLoS ONE* 3: e3479.
16. Müller I (2008) Entropy and energy, - a universal competition. *Entropy* 10: 462-476.
17. Szilárd L (1929) On the decrease of entropy in a thermodynamic system by the intervention of intelligent beings. *Z Phys* 53: 840-856.
18. Landauer R (1961) Irreversibility and heat generation in the computing process. *J Res Dev* 5: 183-191.
19. Bennett CH (1982) The thermodynamics of computation-a review. *Int J Theor Phys* 102: 905-940.
20. Toyabe S, Sagawa T, Ueda M, Muneyuki E, Sano M (2010) Experimental demonstration of information-to-energy conversion and validation of the generalized Jarzynski equality. *Nature Physics* 6: 988-992.
21. Mandal D, Jarzynski C (2012) Work and information processing in a solvable model of Maxwell's demon. *PNAS* 109: 11641-11645.
22. Fermi E, Pasta J, Ulam S (1955) Studies of nonlinear problems. Los Alamos document LA-1940 27: 379.
23. Antonopoulos C, Bountis T (2006) Stability of simple periodic orbits and chaos in a Fermi-Pasta-Ulam lattice. *Phys Rev E* 73: 056206.
24. Antonopoulos C, Bountis T, Skokos C (2006) Chaotic dynamics of N -degree of freedom Hamiltonian systems. *Int J Bif Chaos* 16: 1777-1793.

25. Abramowitz M, Stegun I (1965) Handbook of mathematical functions. Dover, New York.
26. Rechester AB, Rosenbluth MN, White RB (1979) Calculation of the Kolmogorov entropy for motion along a stochastic magnetic field. *Phys Rev Lett* 42: 1247.
27. Pettini M, Landolfi M (1990) Relaxation properties and ergodicity breaking in nonlinear Hamiltonian dynamics. *Phys Rev A* 41: 768.
28. Pettini M, Cerruti-Sola M (1991) Strong stochasticity threshold in nonlinear large Hamiltonian systems: Effect on mixing times. *Phys Rev A* 44: 975.
29. Pettini M, Casetti L, Cerruti-Sola M, Franzosi R, Cohen EGD (2005) Weak and strong chaos in Fermi-Pasta-Ulam models and beyond. *Chaos* 15: 015106.
30. Benettin G (1984) Power-law behavior of Lyapunov exponents in some conservative dynamical systems. *Physica D* 13: 211-220.
31. Livi R, Politi A, Ruffo S (1986) Distribution of characteristic exponents in the thermodynamic limit. *J Phys A: Math Gen* 19: 2033-2040.
32. Wolf A, Swift JB, Swinney HL, Vastano JA (1985) Determining Lyapunov exponents from a time series. *Physica D* 16: 285.
33. Rugh HH (1997) Dynamical approach to temperature. *Phys Rev Lett* 78: 772-774.
34. Popovski P, Fouladgar A, Simeone O (2013) Interactive joint transfer of energy and information. *IEEE Transactions on Communications* 61.
35. Mohammad Fouladgar A, Simeone O (2013) Information and energy flow in graphical networks with energy transfer and reuse. *IEEE Wireless Communications Letters* PP.
36. Park J, Clerckx B (2013) Joint wireless information and energy transfer in a two-user MIMO interference channel. *CoRR* abs/1303.1693.

Figure Legends

Tables

Figure 1. Schematic representation of the time evolution after one time step dt of two deviation vectors (arrows) corresponding to the direction along the Lyapunov exponent λ_1^{KP} on the 1-dimensional subspace $K + P = E$ on the KP space. $\vec{X}_1(t)$ and $\vec{X}_2(t)$ are two trajectories in the phase space of Hamiltonian (3) that drive the dynamics along this line. We denote with δ and Δ the lengths of the two deviation vectors initially and after one time step, respectively.

Figure 2. Plot of the absolute difference $|\lambda_1 - \lambda_1^{KP}|$ as a function of time for two trajectories $\vec{X}_1(t)$ and $\vec{X}_2(t)$ located initially in the neighborhood of SPO2 at the same energy E . Here, $E = 30$ is well inside the interval (E_U, E_T) . Note that both axes are logarithmic.

Figure 3. Plot of the quantities: I_c as defined by Eq. (18) in red dashed line with points, H_{KS} as defined by Eq. (1) in green dashed line with rectangles, I_c^{KP} as defined by Eq. (19) in black solid line with lower triangles and $\langle |\frac{\Delta K}{dt}| \rangle_t$ as defined by Eq. (21) in blue dashed line with upper triangles as a function of E for initial conditions $\vec{X}(0)$ located in the neighborhood of SPO2 of the FPU system. Note that both axes are logarithmic.

Figure 4. Panel A: Plot of quantities: I_c of Eq. (18) in red dashed line with points and H_{KS} of Eq. (1) in green dashed line with rectangles. Panel B: Plot of quantities $I_c^{KP} = \lambda_1$ with red points with the power-law fitting of Eq. (27) in green line. Panel C: Plot of $\langle |\frac{\Delta K}{dt}| \rangle_t$ with red points with the power-law fitting of Eq. (29) in green line. Panel D: Power-law dependence of $\langle |\frac{\Delta K}{dt}| \rangle_t$ to $I_c^{KP} = \lambda_1$ in red points, in the interval $(0.140, 0.174)$ that corresponds to the energy interval $[30, 47]$ of panels A, B and C and of the power-law fitting of Eq. (29) in green dashed line. Note that all axes are logarithmic.

Figure 5. Panel A: Plot of quantities: I_c as defined by Eq. (18) in red dashed line with points, H_{KS} as defined by Eq. (1) in green dashed line with rectangles, I_c^{KP} as defined by Eq. (19) in black solid line with lower triangles and $\langle |\frac{\Delta K}{dt}| \rangle_t$ as defined by Eq. (21) in blue dashed line with upper triangles as a function of E for initial conditions $\vec{X}(0)$ located in the neighborhood of SPO2 of the FPU system. Note that both axes are logarithmic. Panel B: Plot of $I_c^{KP} = \lambda_1$ with red points with the power-law fitting of Eq. (32) in green line. Panel C: Plot of $\langle |\frac{\Delta K}{dt}| \rangle_t$ with red points with the power-law fitting of Eq. (33) in green line. Panel D: Power-law dependence of $\langle |\frac{\Delta K}{dt}| \rangle_t$ to $I_c^{KP} = \lambda_1$ in red points, in the interval $(0.02, 0.174)$ that corresponds to the energy interval $[3, 47]$ of panels A, B and C and of the power-law fitting of Eq. (33) in green dashed line. Note that all axes are logarithmic.

Figure 6. Panel A: Plot of quantities: I_c as defined by Eq. (18) in red dashed line with points, H_{KS} as defined by Eq. (1) in green dashed line with rectangles, I_c^{KP} as defined by Eq. (19) in black solid line with lower triangles and $\langle |\frac{\Delta K}{dt}| \rangle_t$ as defined by Eq. (21) in blue dashed line with upper triangles as a function of E for initial conditions $\vec{X}(0)$ located in the neighborhood of SPO1 of the FPU system. Note that both axes are logarithmic. Panel B: Plot of $I_c^{KP} = \lambda_1$ with red points with the power-law fitting of Eq. (32) in green line. Panel C: Plot of $\langle |\frac{\Delta K}{dt}| \rangle_t$ with red points with the power-law fitting of Eq. (33) in green line. Panel D: Power-law dependence of $\langle |\frac{\Delta K}{dt}| \rangle_t$ to $I_c^{KP} = \lambda_1$ in red points, in the interval $(0.07, 1)$ that corresponds to the energy interval $[10, 10^4]$ of panels A, B and C and of the power-law fitting of Eq. (33) in green dashed line. Note that all axes are logarithmic.

Figure 7. Panel A: Plot of quantities: I_c as defined by Eq. (18) in red dashed line with points, $H_{\mathbf{KS}}$ as defined by Eq. (1) in green dashed line with rectangles, I_c^{KP} as defined by Eq. (19) in black solid line with lower triangles and $\langle |\frac{\Delta K_1}{dt}| \rangle_t$ as defined by Eq. (22) in blue dashed line with upper triangles as a function of E for initial conditions $\vec{X}(0)$ located in the neighborhood of the OPM of the BEC Hamiltonian. Note that both axes are logarithmic. Panel B: Plot of $(\lambda_1 - \lambda_2)$ with red points with the power-law fitting of Eq. (32) in green line. Panel C: Plot of $\langle |\frac{\Delta K_1}{dt}| \rangle_t$ with red points with the power-law fitting of Eq. (33) in green line. Panel D: Power-law dependence of $\langle |\frac{\Delta K_1}{dt}| \rangle_t$ to $(\lambda_1 - \lambda_2)$ in red points, in the interval (0.02, 0.57) that corresponds to the energy interval (3.94, 1037.56) of panels A, B and C and of the power-law fitting of Eq. (33) in green dashed line. Note that all axes are logarithmic.

Figure 8. Panel A: Plot of the quantity I_c as defined by Eq. (18) in red dashed line with points, $H_{\mathbf{KS}}$ as defined by Eq. (1) in green dashed line with rectangles, I_c^{KP} as defined by Eq. (19) in black solid line with lower triangles and $\text{MIR}_{1,14}$ in blue dashed line with upper triangles as a function of E for initial conditions $\vec{X}(0)$ set in the neighborhood of SPO2. Panel B: Same as in panel A for initial conditions set in the neighborhood of SPO1. Note that all axes are logarithmic.